5. ALKALI-METAL CORROSION STUDIES

W. O. Harms J. H. DeVan A. P. Litman

The purpose of this program is to investigate the chemical and metallurgical effects produced in structural materials during exposure to alkali metals. The program is designed to guide the selection of container materials for Na-cooled fast breeder reactor systems and Li-cooled space power reactor systems in which K serves as the Rankine-cycle working fluid. Forced circulation loops of engineering scale are included in the latter program.

Studies of the Corrosion of Vanadium Alloys in Sodium

Although V alloys are highly resistant to dissolution by Na, they are quite reactive with nonmetallic impurities in Na, particularly with C, N, and O. Accordingly, we are investigating the mechanisms by which V alloys are attacked in Na at impurity levels typical of service conditions in a reactor. Our program is concerned with four basic aspects of the oxidation process for V alloys in Na: (1) the partitioning of O between V alloys and Na; (2) the effects of alloying additions of Cr and Zr on the diffusion coefficient of O in V; (3) the effects of Cr and Zr in V on the oxide formed and on the dissolution of the alloys in Na; and (4) the solubility of V in Na as affected by the presence of O in either metal. We are also examining the kinetics of the transfer of C, N, and O between V alloys and types 304 and 321 stainless steel in a Na circuit.

Effects of Oxygen on the Compatibility of Vanadium and Sodium (R. L. Klueh)

We are continuing our study of the processes involved in the interaction of the O in Na with unalloyed V. Vanadium specimens exposed to Na in Mo and type 304 stainless steel capsules[1,2] were analyzed by

---

[1]R. L. Klueh, Fuels and Materials Development Program Quart. Progr. Rept. Dec. 31, 1968, ORNL-4390, p. 85.

[2]R. L. Klueh, Fuels and Materials Development Program Quart. Progr. Rept. March 31, 1969, ORNL-4420, pp. 89–90.

DISCLAIMER

fast-neutron activation analysis for changes in O concentration. With this method we can analyze the entire specimen, and since the method is nondestructive, the same specimen can be analyzed both before and after exposure to Na. Furthermore, it is possible to remove any external scale and again determine the O concentration.

The results of these analyses are shown in Table 5.1. A dark, external scale was observed on the specimens,[1] and removal of the scale

Table 5.1. Change in Oxygen Concentration in Vanadium Specimens Exposed to Sodium Containing Various Amounts of Oxygen at 600°C

Time of Na Exposure (hr)	Initial O Content[a] of Na (ppm)	O Concentration[b] in V, ppm		
		Before Test	After Test	
			With Scale	Without Scale
		Mo Container		
100	2000	1238	4120	3307
200	1800	1236	4081	3360
300	1950	1219	5763	4742
400	1950	1328	5340	c
500	1800	1273	5780	c
500	50	1290	1422	1217
500	450	1233	2953	2723
500	1000	1294	4354	3695
500	4000	1297	6155	c
		Type 304 Stainless Steel Container		
100	2000	1220	4386	2934
200	2050	1314	4899	3195
300	2050	1267	6165	3910
400	2050	1250	5203	c
500	2050	1271	6206	c
500	50	1267	1466	1253
500	550	1229	3038	2343
500	1100	1308	4633	3438
500	4000	1188	9793	c

[a] Oxygen was added as Na_2O.

[b] Oxygen concentrations were determined by fast-neutron activation analysis.

[c] Specimen was sectioned for chemical analysis of the external film.

in all cases lowered the O content. Measurements of the thickness of the specimens showed the scale to be about 0.0005 in. thick. The measured changes in O content in these specimens generally agree with the measurements[1] of weight gain (i.e., the percentage of the O picked up by the V specimen decreased as the O in the Na increased). The decrease was quite significant in the case of the Mo capsules: the V specimen picked up only 50% of the 4000 ppm O addition compared to 75% of the 2000 ppm addition and essentially 100% of all lower additions. For the type 304 stainless steel capsules, on the other hand, similar calculations showed that essentially all of the O in the Na was gettered by the V specimen. More than 95% of the O was accounted for in all but the test that contained 4000 ppm O, where about 93% was recovered.

Smith[3] reported the solubility of O in alpha V to be on the order of 1.2 wt % at 600°C. In a study of the uptake of O by V wires in a stainless steel and Na system, this O saturation level was achieved in Na containing about 0.8 ppm O. These data suggest that the distribution coefficient for partitioning of O between Na and V $\left(\frac{\text{ppm O in V}}{\text{ppm O in Na}}\right)$ is on the order of 1.5×10^4. In our stainless steel capsule tests, we did not directly determine the O content in the Na after test, however, we did calculate the O content by means of a mass balance on O. The results showed that the distribution coefficient for O approached 10^4.

Attempts to determine the nature of the dark, external scale by x-ray diffraction were unsuccessful – probably because the film was too thin. We analyzed the V specimens to determine if there had been dissimilar-metal mass transfer from the containers. The Mo concentration of the V tested in Mo capsules increased from an initial concentration of less than 10 ppm to about 700 ppm, and the V exposed to Na in stainless steel increased from 80 ppm Fe and < 10 ppm Ni to about 200 ppm Fe and 100 ppm Ni. No other stainless steel components were detected. Considering that Mo, Fe, and Ni will not diffuse into the V to any extent at 600°C, the surface concentrations of the capsule materials – especially Mo – must have increased considerably. The deposition of the Mo on the V

---

[3]D. L. Smith, Reactor Development Program Progress Report, February 1969, ANL-7553, p. 83.

may account for the decrease in the percentage of O recovered at the higher O concentrations.

Finally, the Na was analyzed after test to determine the concentrations of V and container materials present. These results are shown in Tables 5.2 and 5.3.

Mass Transfer of Interstitial Impurities Between Vanadium Alloys and Types 304L and 321 Stainless Steel in Sodium (J. H. DeVan, D. H. Jansen)

The first loop in this series, which is constructed of type 304 stainless steel and unalloyed V, continues to operate at the design conditions.[4] The test, scheduled for 3000 hr, had completed 1700 hr as of July 1. The vacuum atmosphere protecting the loop has steadily improved and the pressure has decreased to about 10^{-10} torr.

A second test loop with type 321 instead of type 304 stainless steel sections was fabricated and is being prepared for operation under conditions similar to those for the first loop.

As discussed previously,[4] we intend to compare the rates of interstitial transport in these loop systems with those of static, isothermal systems. Therefore, we have also begun a series of static tests in which tensile specimens of V sheet are being exposed to Na in stainless steel containers. A schematic of the test system is shown in Fig. 5.1. The number of stainless steel spacers and tensile specimens are varied to attain surface-area ratios that correspond to those in our loop systems. Two such static tests were conducted for 500 hr at 800°C with type 304L stainless steel spacers and containers. Two different grades of V were exposed, one containing 2270 ppm and the other 110 ppm total interstitial impurities. Past test analyses of the interstitials and tests of mechanical properties are still incomplete; however, the V showed consistent weight gains together with a distinct darkening of surfaces (Fig. 5.2). Additional capsule test systems are being fabricated with type 321 stainless steel spacers and containers.

---

[4]J. H. DeVan and D. H. Jansen, Fuels and Materials Development Program Quart. Progr. Rept. March 31, 1969, ORNL-4420, pp. 90–92.

Table 5.2. Concentrations of Vanadium and Molybdenum in Sodium After Exposure of Vanadium Coupons in Molybdenum Capsules at 600°C

Exposure Time (hr)	Initial O Content of Na (ppm)	Concentration of Metal in Na, ppm	
		V	Mo
100	2000	12	230
200	1800	7	290
300	1950	8	240
400	1950	18	290
500	1800	32	
500	50	6	
500	450	5	
500	1000	8	
500	4000	68	

Table 5.3. Concentrations of Vanadium, Iron, Nickel, and Chromium in Sodium After Exposure of Vanadium Coupons in Stainless Steel Capsules at 600°C

Exposure Time (hr)	Initial O Content of Na (ppm)	Concentration of Metal in Na, ppm			
		V	Fe	Ni	Cr
100	2000	7	100	3	10
200	2050	13	130	2	90
300	2050	3	35	1	2
400	2050	12	95	3	8
500	2050	19			
500	50	0.2			
500	550	16			
500	1100	16			
500	4000	25			

ORNL-LR-DWG 46643R3

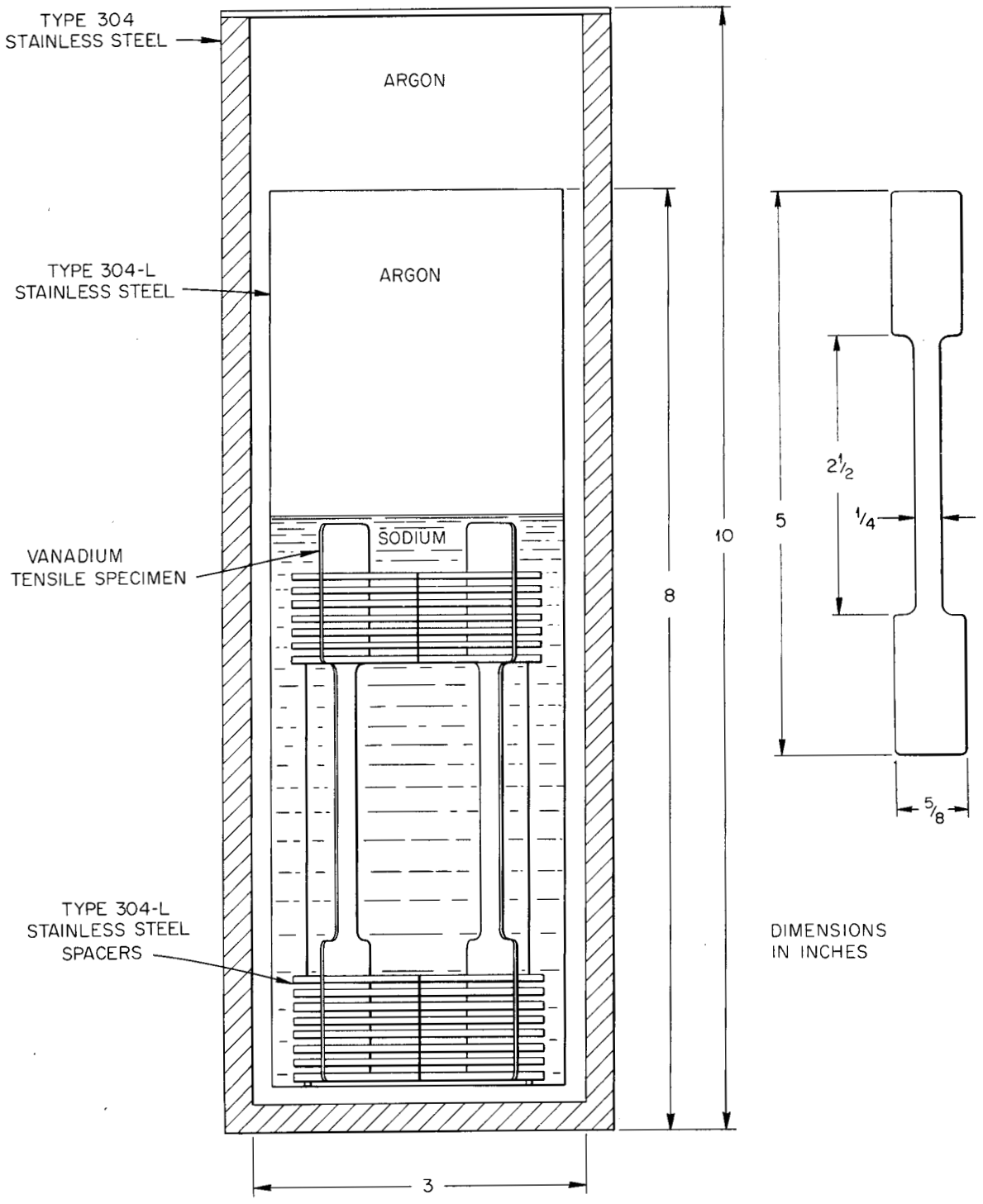

Fig. 5.1. Schematic Drawing of Static Test System Used to Study Dissimilar-Metal Mass Transfer Between Vanadium and Stainless Steel.

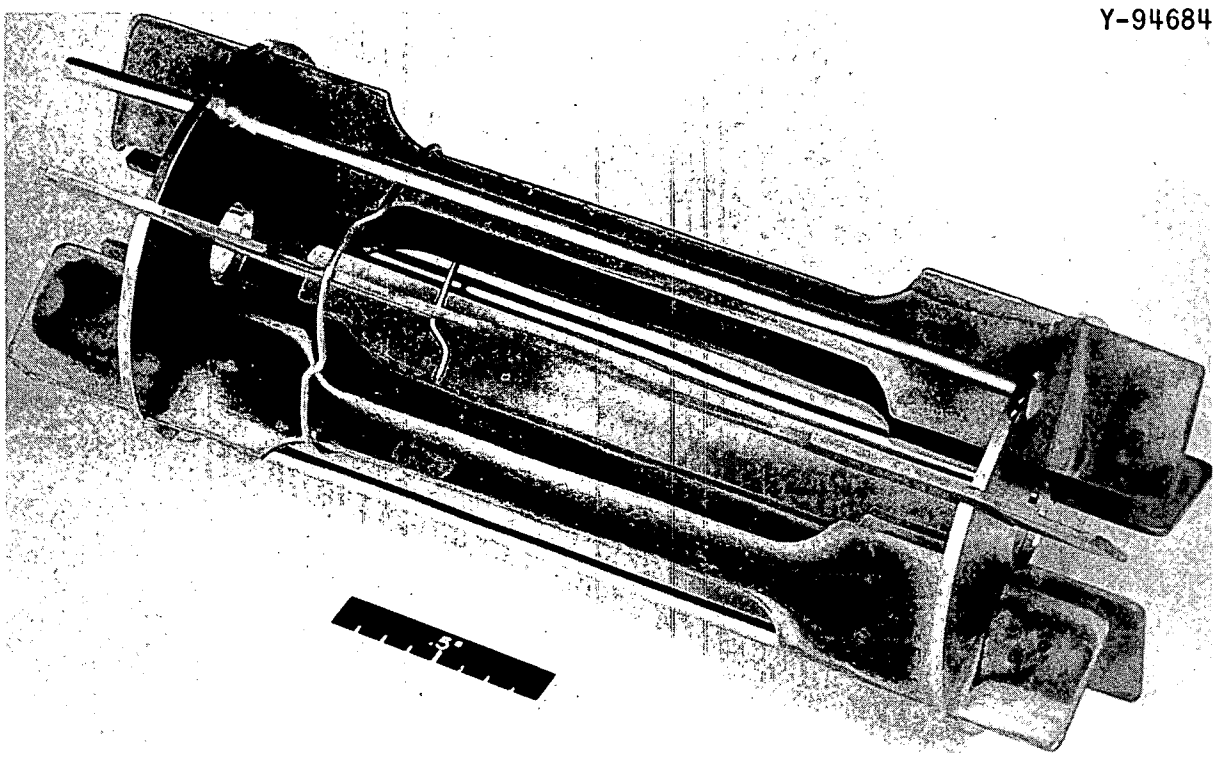

Fig. 5.2. Tensile Specimens of Vanadium Sheet After 500-hr Static Test at 800°C.

Interstitial Contamination of Vanadium and Its Alloys (R. L. Wagner)

We are studying the interaction of V with gaseous interstitial impurities to characterize any effect of alloying additions in V on the rate and nature of interstitial contamination and to determine the creep strength of V and its alloys as influenced by interstitial contamination.

Table 5.4 shows the effect of a 100-hr exposure on the interstitial content of V at 900°C under various vacuum conditions. For the pressure range studied, 10^{-5} to 10^{-7} torr, N and C remained unchanged. However, O increased by 150 ppm at 6×10^{-6} torr and by 220 ppm at 1.6×10^{-5} torr, but when the sample was wrapped in Ta foil there was no contamination even at 1.6×10^{-5} torr. For pressures below 10^{-7} torr, contamination by residual gases at 900°C does not appear to be a problem.

Table 5.4. Effect of Vacuum Exposure on the Interstitial Content of Vanadium[a] at 900°C for 100 hr

Pressure (torr)	Interstitial Content,[b] ppm		
	C	N	O
As received	320	530	210
4×10^{-7}	320	520	220
6×10^{-6}	260	540	360
1.6×10^{-5}	320	530	430
1.6×10^{-5}[c]	300	530	220

[a] Vanadium foil 0.015 in. thick.

[b] Chemistry determined by vacuum-fusion analysis.

[c] Wrapped with Ta foil.

Table 5.5 shows the results obtained to date on the contamination of V at controlled O pressures. At a base pressure of 4×10^{-8} torr, little interstitial change was noted after 810 hr. At 2×10^{-7} torr and at 2×10^{-6} torr O, the rate of O pickup was maximum at about 550°C.

As shown below,[5] increasing concentrations of interstitial elements significantly increase the yield strength of pure V at 0°C:

Concentration, ppm	Upper Yield Stress, psi $\times 10^3$
120 C	12
1000 C	20
120 N	12
1000 N	50
120 O	12
1000 O	37

[5] D. R. Matthews et. al., Effects of Interstitial Impurities on the Mechanical Properties of Electrorefined Vanadium at Low Temperatures, U.S. Bureau of Mines Report 6637 (1965).

Table 5.5. Oxygen Contamination of Vanadium[a,b]

4×10^{-8} torr Vacuum, 810 hr		2×10^{-7} torr O_2, 500 hr		2×10^{-6} torr O_2, 200 hr	
Temperature (°C)	Change in $_c^O$ Concentration in V (ppm)	Temperature (°C)	Change in $_c^O$ Concentration in V (ppm)	Temperature (°C)	Change in $_c^O$ Concentration in V (ppm)
410	−6	450	+45	370	+28
520	+9	550	+240	460	+388
615	+60	670	+200	560	+478
730	+3	775	+155	670	+358
810	+18	850	+100	745	+308
810	+30	810	+95	780	+218
890	+24	905	+100	830	+268

[a]Results based on specimens 0.020 in. thick with surface area of 7.595 in.^{2}.

[b]Material tested after a 1-hr anneal at 900°C in $< 1 \times 10^{-6}$ torr vacuum.

[c]Chemistry changes determined by vacuum-fusion analysis.

Data on the effects of interstitials on the creep strength of V and its alloys are largely lacking, and an apparatus has been designed to obtain creep data under conditions of controlled contamination.

Compatibility of Stainless Steel and Insulation in LMFBR Systems

C. D. Bopp A. P. Litman

Since the compatibility of insulating materials with stainless steels is an important consideration in the design of LMFBR systems, we are studying the reactions that can occur between commercial insulating materials and stainless steel.

The first phase of our program is concerned with the interactions of stainless steels and commercial alumina-silica insulation materials at temperatures between 370 and 760°C. The second phase deals with the effects of Na leaks in stainless steel systems surrounded by thermal insulation. Small leaks that may be self-sealing at lower temperatures are being studied by methods similar to those used in the first phase of this task. The effect of large leaks will be studied in heated, pressurized containers with artificial defects incorporated into the container wall.

Except for some continuing long-term tests, we have completed our experimental study of the compatibility of insulation with stainless steel in the absence of Na oxidation products.[6,7] We are now assembling the equipment to be used in the second phase of this program, which deals with the effect of a Na leak.

Effect of Insulation on Oxidation of Stainless Steel

We have completed a metallographic examination of tubes of types 304L and 316 stainless steel exposed to moist air at 730 to 815°C (ref. 7). In

---

[6]C. D. Bopp, Fuels and Materials Development Program Quart. Progr. Rept. Dec. 31, 1968, ORNL-4390, pp. 91–92.

[7]C. D. Bopp, Fuels and Materials Development Program Quart. Progr. Rept. March 31, 1969, ORNL-4420, pp. 92–100.

these tests, about one-half of both the inside and outside surfaces of the specimens contacted fibrous "blanket-grade" alumina-silica insulation. The effect of the insulation on scaling was assessed by metallographic comparison of the bare and insulated parts.

In the case of type 304L stainless steel, the surfaces in contact with insulation developed a dull, rusty-red scale, and those away from the insulation developed a shiny, blue-gray scale [Fig. 5.3(a)]. The metallographic appearance of the uninsulated surfaces is shown in [Fig. 5.3(b)]. Note the small mounds, which are characteristic of breakaway oxidation.[8] The features of the underlying scale on the insulated part were obscured by a very thin surface layer of rusty-red, powdery Fe_2O_3. However, the larger mounds evident in this underlying scale [Fig. 5.3(e) and (f)] closely resembled those of the uninsulated sections [Fig. 5.3(c) and (d)]. The averages of a large number of measurements of scale thickness did not show a significant difference between the insulated and bare parts or between the inner and outer surfaces.

The formation of mounds is characteristic of breakaway oxidation, and the kinetic data from these tests indicated a slow acceleration in weight gain. Nevertheless, the rate of oxidation was relatively low at the time this run was terminated (1200 hr). We believe that the powdery Fe_2O_3 layer on only the insulated part resulted from abrasion of the scale by the insulation. However, this effect should not be particularly deleterious under LMFBR conditions since it was confined to a very thin surface layer, and in these tests the insulation was compressed against the tubes much more than it is in usual insulation practice.

Kinetic data from these tests[7] indicated that the oxidation resistance of type 316 stainless steel was substantially less than that of type 304L stainless steel. Metallographic examination of the type 316

---

[8]L. A. Morris, Metals. Eng. Quart. 8(2) 30 (May 1968).

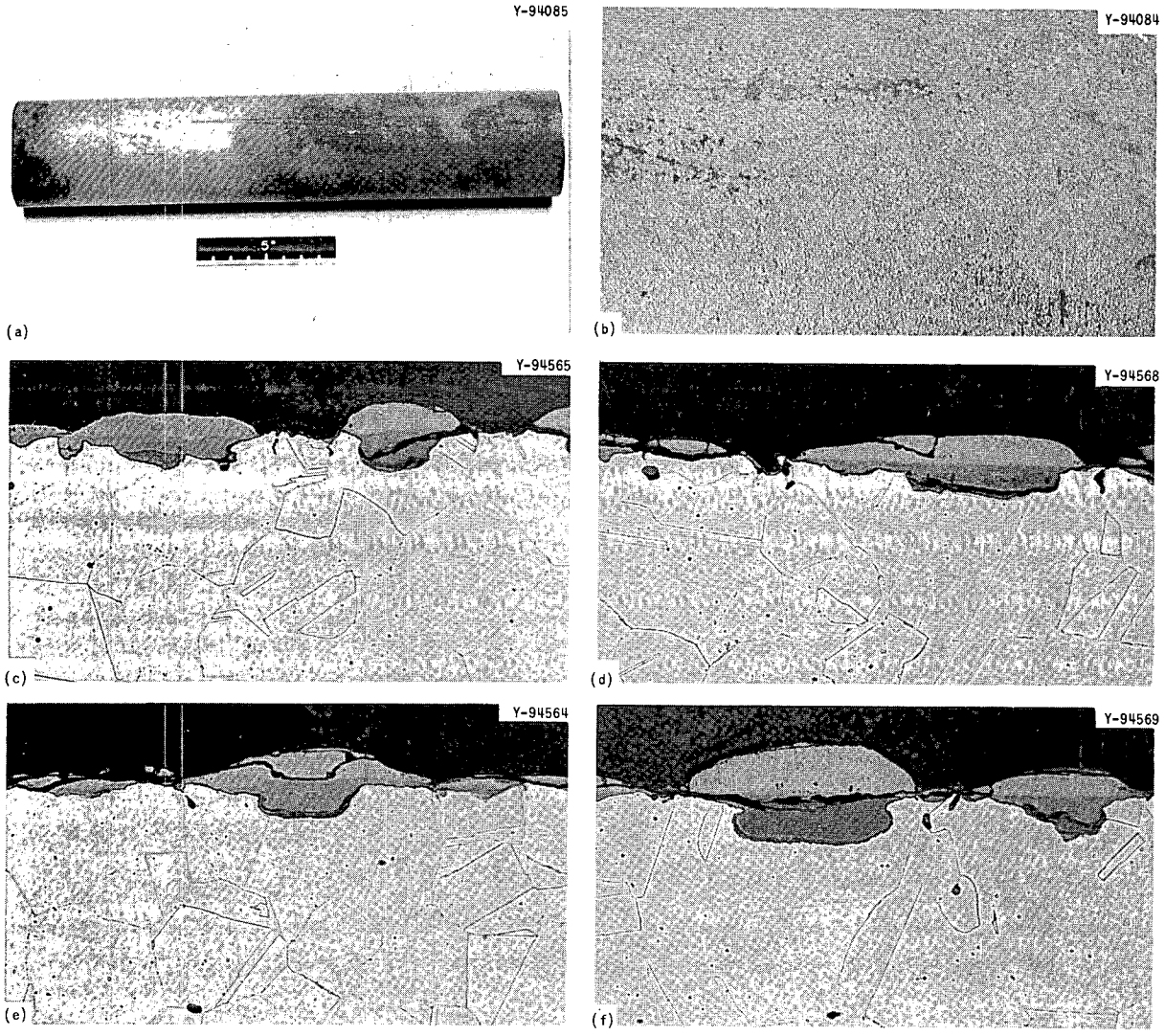

Fig. 5.3. Appearance of Type 304L Stainless Steel Oxidized 1200 hr at 760°C in Moist Air (Saturated at 20°C) and Temperature Cycled to 200°C Every 40 hr. (a) Outer surface. (b) Outer surface of bare end. 10×. (c) Section of outer surface of bare end. Etchant: lactic, nitric, and hydrochloric acid. 500×. (d) Section of inner surface of bare end. 500×. (e) Section of outer surface of insulated end. 500×. (f) Section of inner surface of insulated end. 500×. Reduced 48.5%.

stainless steel specimens showed that the scale rapidly achieved a thickness at which it spalled because of the stresses produced by growth. (A theory of such spalling has been advanced in the instance of Zr alloys.[9]) Spalling, as shown in Fig. 5.4(a) and (b), exposes a dark, relatively adherent inner layer. Although the thickness of the adherent scale was not very uniform, there was no consistent difference between the insulated [Fig. 5.4(c) and (d)] or bare [Fig. 5.4(e) and (f)] parts or the outer [Fig. 5.4(c) and (e)] or inner [Fig. 5.4(d) and (f)] surfaces of the tube.

An electron microprobe trace was obtained across the scale formed on type 316 stainless steel oxidized for 650 hr at 150 to 815°C in moist air (Fig. 5.5). The limitations with regard to resolution of the microprobe method were discussed by Brush[10] who showed that the effective limit is a diameter of about 3 μm. It is only possible to locate the interfaces approximately because of roughness. The composition of the outer layer of scale corresponds roughly to Fe_3O_4 (72% Fe); the composition of the inner layer suggests a mixture consisting principally of $FeCr_2O_4$ and $NiFe_2O_4$. The phase composition is being determined by x-ray diffraction.

We conclude from the metallographic and kinetic[7] studies of scaling that with type 304L stainless steel to 760°C there is little effect of contact with blanket-grade insulation and that even after breakaway oxidation the scaling rate is very low. With type 316 stainless steel, again there is little effect of the insulation; however, the scale formed at 760°C is much less protective. This accords with the finding by others[8] that aging at 760°C enhances corrosion in superheated steam. The similarity between corrosion in air and steam is further demonstrated by comparison of our electron microprobe trace with that for corrosion in steam.[11]

---

[9]J. C. Greenback and S. Harper, Electrochem. Technol. 4, 88 (1966).

[10]E. G. Brush, Oxidation Behavior of Fe-Cr-Ni System in High-Pressure Steam, GEAP-4490 (March 1964).

[11]George E. Lien, ed., Superheater Alloys in High Temperature, High Pressure Steam, The American Society of Mechanical Engineers, New York, N. Y., 1968.

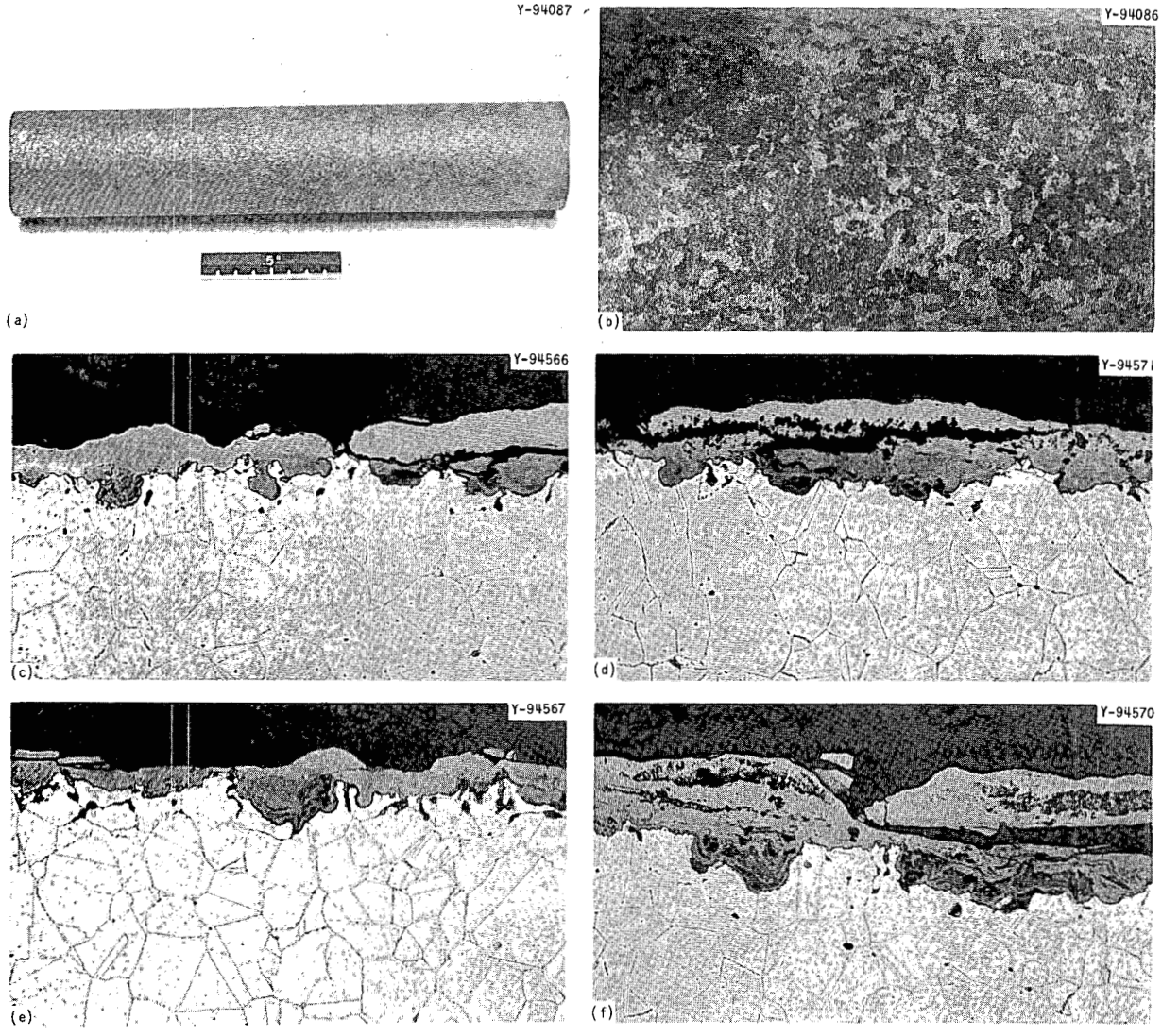

Fig. 5.4. Appearance of Type 316 Stainless Steel Oxidized 550 hr at 760°C in Moist Air (Saturated at 20°C) and Temperature Cycled to 200°C Every 40 hr. (a) Outer surface. (b) Outer surface of bare end. 5×. (c) Section of outer surface of bare end. 500×. (d) Section of inner surface of bare end. 500×. (e) Section of outer surface of insulated end. 500×. (f) Section of inner surface of insulated end. 500×. Reduced 48.5%.

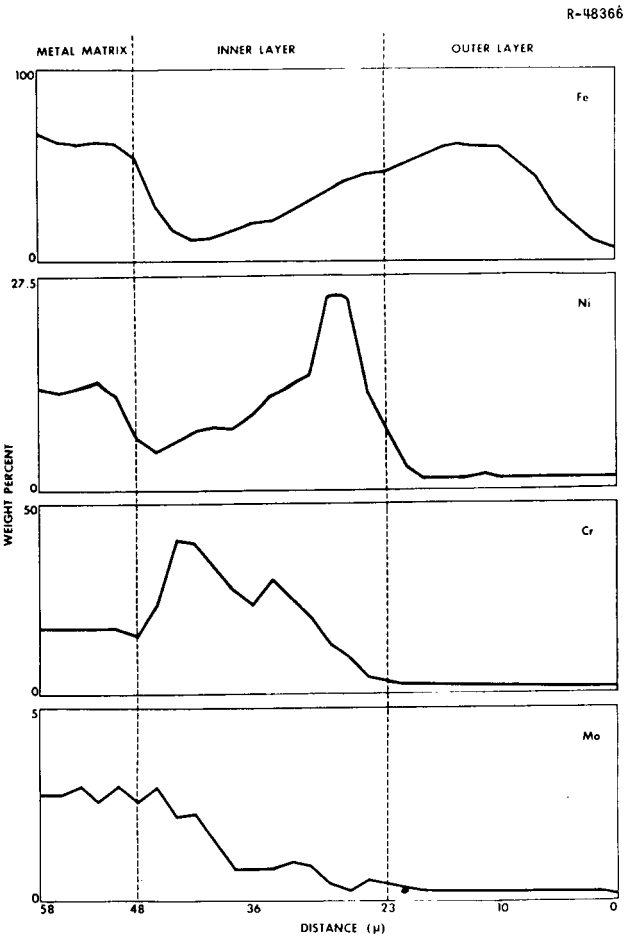

Fig. 5.5. Electron Microprobe Trace of Adherent Scale on Type 316 Stainless Steel After 650 hr at 815°C with Temperature Cycled to 150°C Every 6 hr in Moist Air (Saturated at 20°C).

Corrosion of Refractory Alloys in Lithium, Potassium, and Sodium

J. H. DeVan A. P. Litman W. R. Huntley

Requirements for auxiliary electricity or ion propulsion for space vehicles necessitate power plants of high efficiency that will operate at high temperatures. For these applications, nuclear power systems have been proposed in which alkali metals are used to transfer heat, drive a turbogenerator, and lubricate rotating components. Accordingly, we are investigating the corrosion properties of candidate alkali metals, primarily Li and K, under conditions of interest for space applications. Because of the relatively high temperatures (> 1000°C), the investigation is concerned largely with refractory-metal container materials.

Effect of Oxygen on Compatibility of Refractory Metals and Alkali Metals (R. L. Klueh)

Oxygen Effects in the Niobium-Lithium and Tantalum-Lithium Systems. — We completed comparative studies[12–14] of the effects of O in various refractory metal-alkali metal systems at 600°C. The final tests in this series dealt with the Nb-O-Li and Ta-O-Li systems. In five tests of each system, nominally pure capsules and specimens were exposed to Li with varying additions of Li_2O. Two other capsules of each material were also tested with specimens to which O had been added before test.

The weight changes of the specimens are shown in Table 5.6. The O concentration of the Li did not measurably affect the amount of Nb or Ta dissolved by the Li. For both systems, the amount of metal in the Li after test was less than the limit of detection (< 10 ppm O). This is quite different from what we found for Nb and Ta in K or Na; there we found that the amounts of Nb and Ta dissolved were highly dependent upon the O concentration in the liquid metal.[12–14]

When O was added to the Nb or Ta specimens, the attack by Li with a given O level was much more severe than that by K (ref. 12) or Na (refs. 13 and 14). Figure 5.6 shows the after-test appearance of Ta that contained 1100 ppm O before exposure to Li. We noted large amounts of transgranular attack by Li in both Ta and Nb under conditions that produced only grain boundary attack by Na and K. As was true of the attack by K and Na, Li also attacked Ta more severely than it attacked Nb.

The greater susceptibility of Ta to attack was further substantiated by the appearance of the Ta capsules. When the Ta capsules were removed from the stainless steel outer containers that enclosed them during the

[12]R. L. Klueh, Fuels and Materials Development Program Quart. Progr. Rept. Sept. 30, 1968, ORNL-4350, pp. 120–126.

[13]R. L. Klueh, Fuels and Materials Development Program Quart. Progr. Rept. Dec. 31, 1968, ORNL-4390, p. 95.

[14]R. L. Klueh, Fuels and Materials Development Program Quart. Progr. Rept. March 31, 1969, ORNL-4420, pp. 100–103.

Table 5.6. Effect of Oxygen on the Compatibility of Niobium and Lithium and Tantalum and Lithium

Test Material	Initial O Concentration[a] in Li (ppm)	O Concentration[b] in Refractory Metal, ppm		Specimen Weight Change[c] (mg)
		Before Test	After Test	
Nb	100	70	47	+0.1
	600	70	57	0.1
	1100	70	49	0.1
	1600	70	41	0.1
	2100	70	49	0.1
	100	1100	490	−0.6[d]
	100	2200	1400	−14.4[d]
Ta	100	40	59	0.0
	600	40	29	0.0
	1000	40	37	0.0
	1600	40	32	0.0
	2100	40	27	0.0
	100	1100	170	−3.4
	100	1900	340	−5.0

[a] Oxygen added as Li_2O to Li containing about 100 ppm O.

[b] Determined by vacuum-fusion analysis.

[c] Specimen size: 1 × 0.5 × 0.04 in.

[d] Specimen was quite brittle and broke during removal from the container; therefore, the measured weight loss is probably high.

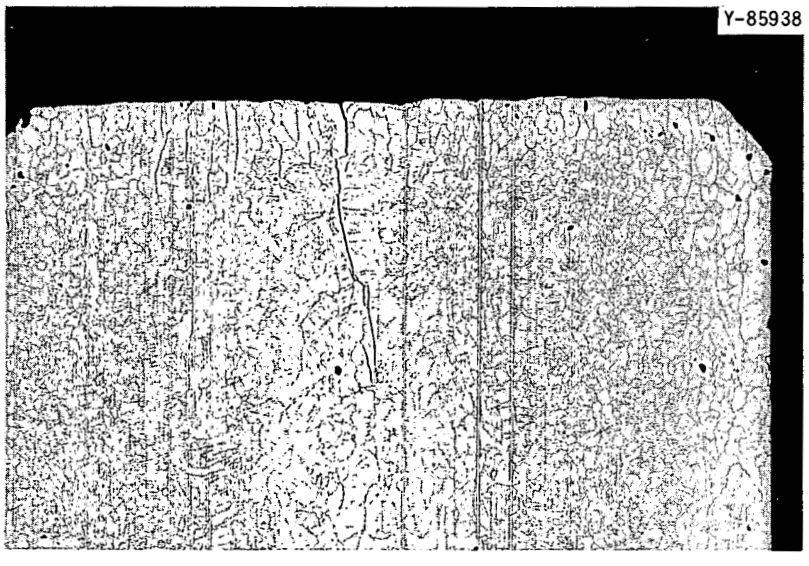

Fig. 5.6. Tantalum That Initially Contained 1100 ppm O After Exposure to Lithium for 500 hr at 600°C. Lithium attacked grain boundaries and produced transgranular platelets. 100×. Reduced 30%.

600°C exposure, they were discolored, and there was evidence of Li around them. Since we could detect no macroscopic failures, we concluded that, although the Ta tubing had contained only 150 to 200 ppm O, Li had penetrated the walls. This was confirmed when the tube walls were sectioned and examined metallographically (Fig. 5.7).

Partitioning of Oxygen Between Potassium and Zirconium and Sodium and Zirconium (R. L. Klueh)

Frequently, Na and K are purified of O by exposing them to Zr in a stainless steel system (either static or dynamic). In view of the inhibiting layers observed on Zr after exposure in Mo capsules,[15] we conducted a series of O partitioning tests of Zr at 815°C in type 304 stainless steel containers to measure dissimilar-metal mass transfer.

[15]R. L. Klueh, Fuels and Materials Development Program Quart. Progr. Rept. Dec. 31, 1968, ORNL-4390, p. 97.

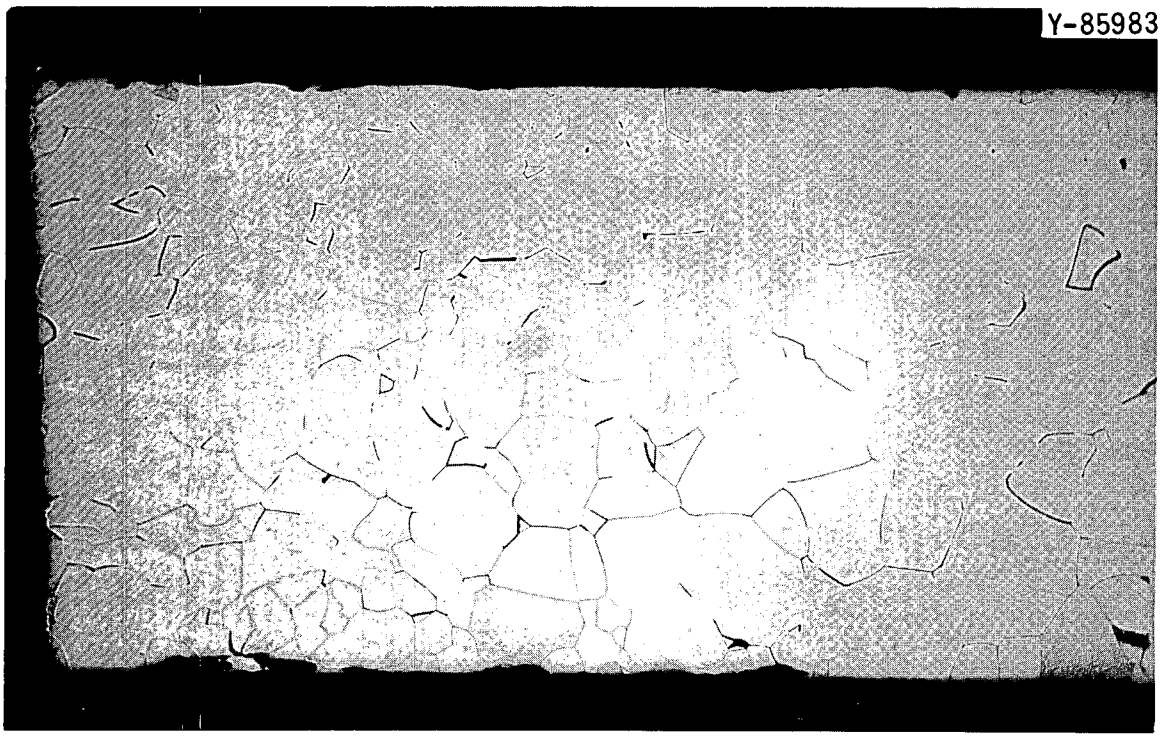

Fig. 5.7. Wall of Tantalum Capsule That Was Exposed to Lithium for 500 hr at 600°C. The tantalum contained about 200 ppm O before test.

We also hoped to explain the anomalous observation that, when purifying Na and K for our loop experiments, 50 to 100 ppm O sometimes remain in the liquid metals even after 100-hr exposures to Zr at 815°C in stainless steel containers.

Results of these recovery experiments are shown in Table 5.7. The percentage of O recovered decreased as the O concentration in the alkali metal increased. (Recoveries greater than 100% are apparently the result of O transfer from the stainless steel.) In all cases, the Zr specimens

Table 5.7. Oxygen Recovered by Zirconium in Type 304 Stainless Steel Containers[a]

O in K, ppm		O in Na, ppm	
Total[b]	Recovered	Total[c]	Recovered
600	700	450	530
930	800	990	920
1330	1250	1350	1300
1680	1400	1650	1460
2890	2300	2900	1890

[a]All tests were at 815°C for 100 hr with 0.04-in.-thick Zr specimens.

[b]Initial O plus that added as K_2O.

[c]Initial O plus that added as Na_2O.

developed a surface scale that became thicker with increasing O concentration in the alkali metal. Microprobe analysis showed that the scale contained Fe, Mn, and C. In addition, vacuum-fusion analysis showed that O, N, and H had transferred from the stainless steel to the Zr. No intermetallics or other compounds could be identified by x-ray diffraction.

These results indicate that the absorption of O by Zr in stainless steel containers can be inhibited by the mass transfer of stainless

steel components. Whether this inhibiting reaction could become a problem in hot traps is not immediately obvious. Hot-trapped systems generally operate below the O and temperature levels employed here, so that both the solubilities and mass-transfer rates of stainless steel components should be considerably reduced. The present results suggest that, whereas a temperature of 800°C greatly enhances the ability of Zr to take up O by diffusion, a lower temperature, maybe 600°C, may be advantageous for avoiding dissimilar-metal poisoning of the Zr.

The results on O gettering by Zr reported during the last five quarters were compiled, and a report was issued.[16]

Refractory Alloy – Lithium Thermal Convection Loop Tests (J. H. DeVan)

We have completed our analysis of thermal convection loop TCL-6R, which circulated Li for 3000 hr at a maximum temperature of 1350°C. The loop was constructed of the Ta alloy T-222 and contained T-222 insert specimens.

Bend tests performed[17] on several insert specimens from this test showed that the toughness of the T-222 specimens had deteriorated significantly in areas of the loop that had been at a temperature between 1220 and 1280°C. These specimens increased slightly in N during Li exposure; bulk specimen analyses showed N contents in the affected areas to range from 90 to 250 ppm. Concentrations of other interstitial impurities were essentially the same as before Li exposure.

We have examined several specimens from this group that completely fractured at a relatively low bend angle. As shown in Fig. 5.8, fracture was intergranular. A specimen adjacent to the one shown in Fig. 5.8 was analyzed incrementally to evaluate the distribution of interstitial impurities (O, N, H) across the specimen. It was cut lengthwise and crosswise into four roughly equivalent samples. Three of the four

---

[16]R. L. Klueh, Oxygen Determination and Purification of Liquid Alkali Metals by Zirconium Gettering, ORNL-TM-2473 (March 1969).

[17]J. H. DeVan, Fuels and Materials Development Program Quart. Progr. Rept. March 31, 1969, ORNL-4420, pp. 105–106.

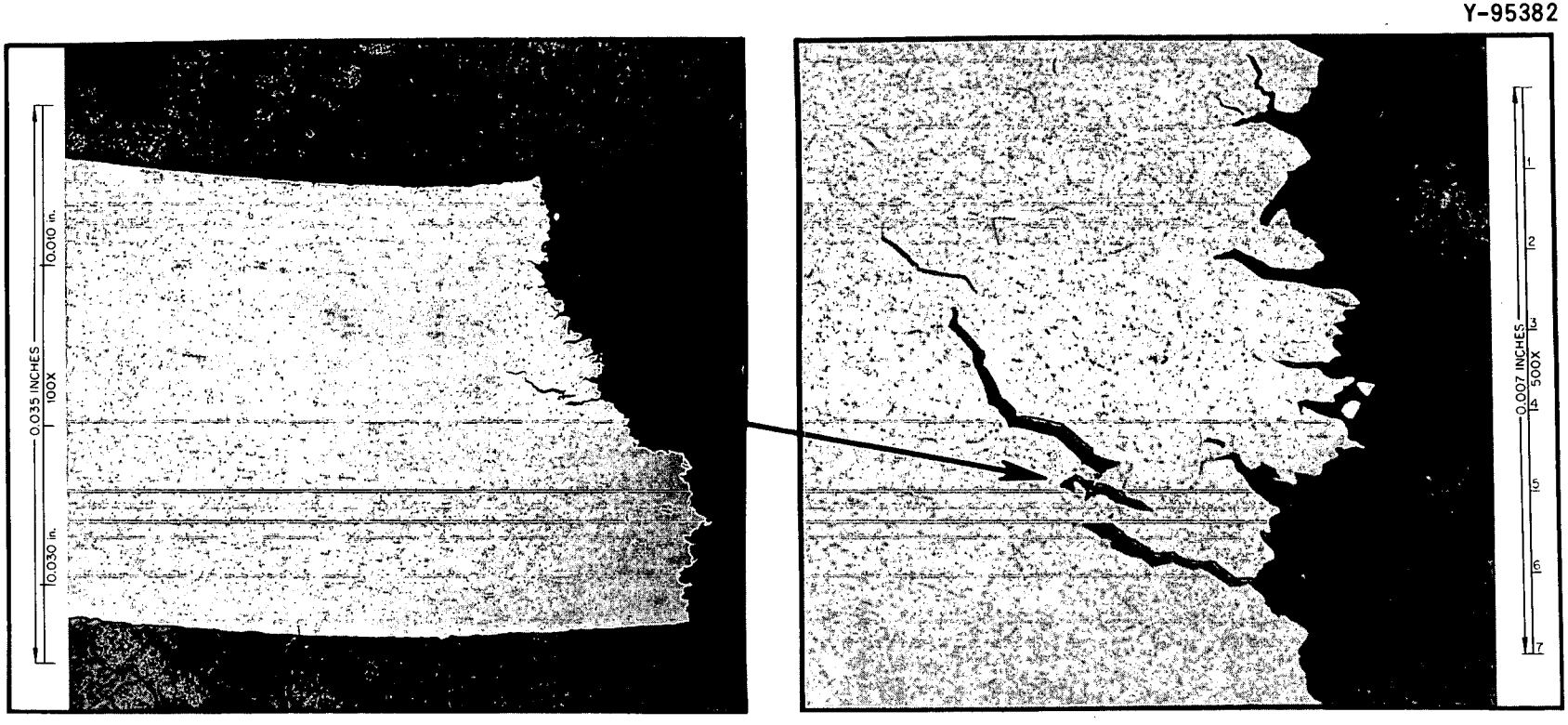

Fig. 5.8. Metallographic Appearance of T-222 Insert Specimen After Bend Test at Room Temperature. Specimen had been exposed to Li for 3000 hr at 1240°C.

samples were then chemically etched[18] to remove varying thicknesses of the outside surface. All four samples were then analyzed by vacuum fusion, and the results are given in Table 5.8. Although there appeared to be some difference in the N content among the four specimens, there was no evidence of a N gradient from the outside to the center of the

Table 5.8. Analyses of T-222 Sheet Specimen[a] Chemically Etched to Remove Varying Surface Layers

Depth of Surface Layer Removed (in.)	Final Thickness of Analytical Specimen (in.)	Concentration of Interstitial Impurities (ppm)		
		O	N	H
Unetched	0.029	22	94	4
0.0020	0.025	28	140	4
0.0045	0.020	25	71	9[b]
0.0095	0.010	38	140	56[b]

[a]Specimen had been exposed to Li for 3000 hr at 1265°C.

[b]Increase in H is attributed to chemical etching used to remove surface layers.

specimen. Oxygen content decreased slightly from the center to the outside, but there was no increment across the specimen where the interstitial impurity level appears abnormally high. Thus, we believe the observed loss in fracture toughness is associated more with the thermal history of these specimens than with changes in interstitial impurities.

T-111 Forced Circulation Liquid Lithium Loop (FCLLL-1) (B. Fleischer, D. L. Clark, C. W. Cunningham)

We completed the final assembly of test loop FCLLL-1. The resistance-heated section of the loop was cycled between ambient

[18]Etchant: 10 H_2SO_4–20 HF–40 HNO_3–30 H_2O (vol %).

temperature and 1370°C before the loop was charged with Li. A trial run was then made at 1370°C with circulating Li. The test was stopped at the end of this report period so that instrumentation and operational difficulties could be investigated and corrected.

Installation of Loop into Vacuum Chamber. – The relative positions of the loop components and piping within the vacuum chamber are shown schematically in Fig. 5.9. Figure 5.10 is a photograph of the resistance heater, economizer, and radiator during an early phase of installation. These components are mounted on a stainless steel frame that is supported from pads fastened to the inner wall of the vacuum-chamber bowl. The

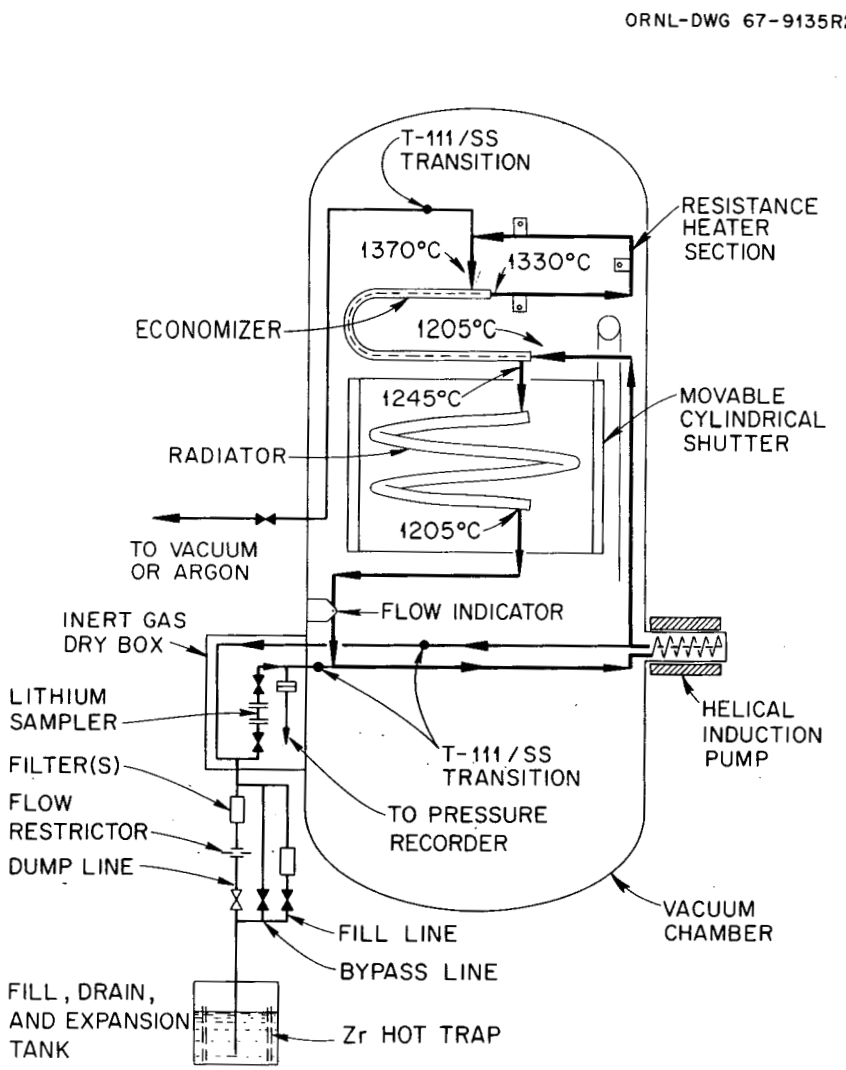

Fig. 5.9. Forced Circulation Liquid Lithium Loop (FCLLL-1).

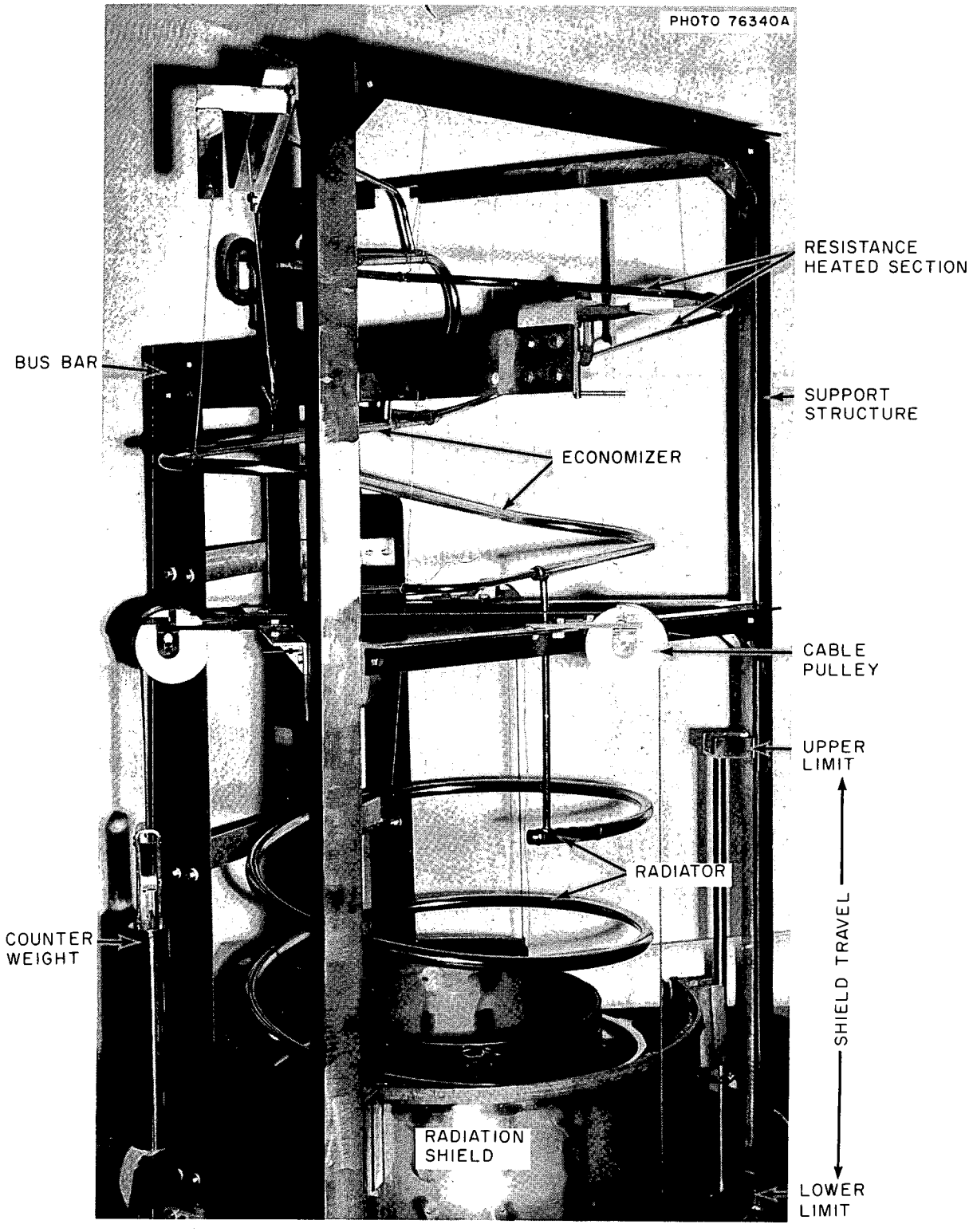

Fig. 5.10. Forced Circulation Liquid Lithium Loop (FCLLL-1) During Installation.

adjustable heat shield surrounding the radiator in Fig. 5.10 is in the position intermediate between its upper and lower limits. This shield is counter weighted so that it can be positioned easily by a magnetically-coupled, rotary feedthrough in the wall of the vacuum chamber. The rotary motion of the feedthrough is transmitted to stainless steel cables that move on alumina pulleys (Fig. 5.10). The pulleys turn on stainless steel shafts that were hard surfaced by welding Stellite-12 on the surface and grinding to finished dimensions. A niobium diselenide lubricant (1-to 2-μm particle size) is also used to avoid galling.

The electrical bus bars delivering current to the resistance heater were made from OFHC-grade Cu. They were coated with high-emissivity iron titanate to increase dissipation of radiation heat.

The loop is shown in Fig. 5.11 as it appeared before its enclosure by the vacuum-chamber bell. All sections of the loop except the radiator were covered by several layers of Ta foil reflective insulation, as shown in this figure. Figure 5.12 shows how the foil was assembled.

The interaction between the atmosphere in the vacuum chamber and the test loop is being monitored by means of two furnace assemblies that are incorporated in the vacuum chamber along with the test loop, as shown in Fig. 5.13. These furnaces are suspended from the support frame above the resistance-heated section of the loop and contain several T-111 sheet specimens. The furnaces consist of W-mesh resistance heaters surrounded by multiple layers of Ta foil reflective thermal insulation. The T-111 control specimens will be held at 1370 and 1225°C, respectively, in a configuration described previously.[19]

Shown in Fig. 5.13 are some of the alumina-insulated bare-wire thermocouples described previously.[20] We also used several sheathed thermocouples to measure the temperatures in the loop. These sheathed thermocouples were made of 0.009-in. sensing wires of the same composition as our bare-wire thermocouples (W–3% Re vs W–25% Re). The outer sheath,

---

[19]D. L. Clark and B. Fleischer, Fuels and Materials Development Program Quart. Progr. Rept. Sept. 30, 1968, ORNL-4350, pp. 131–135.

[20]D. L. Clark, C. W. Cunningham, and B. Fleischer, Fuels and Materials Development Program Quart. Progr. Rept. March 31, 1969, ORNL-4420, pp. 106–113.

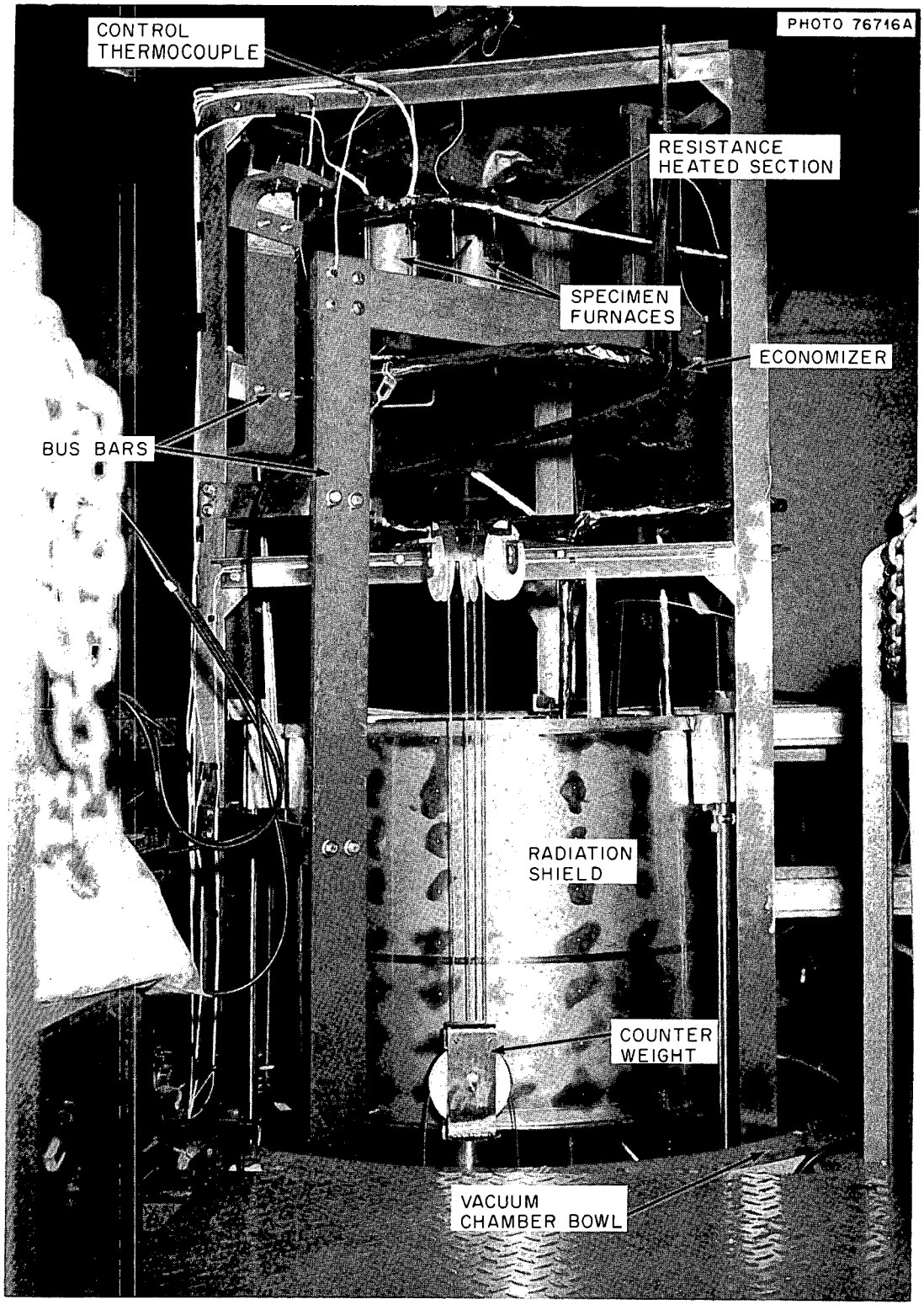

Fig. 5.11. Forced Circulation Liquid Lithium Loop (FCLLL-1) Before Closure of Vacuum Chamber.

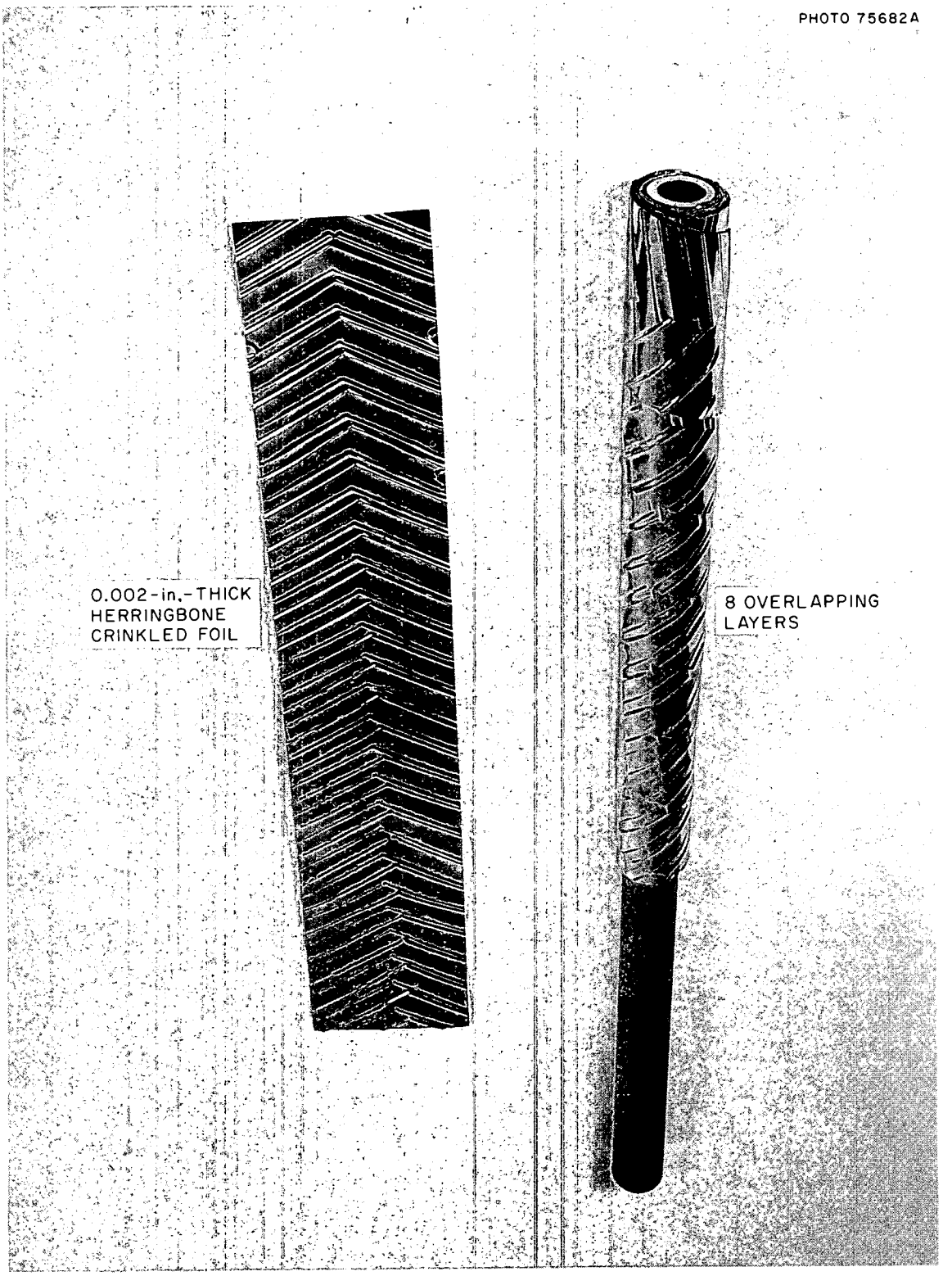

Fig. 5.12. Application of Tantalum Foil Thermal Radiation Insulation for Forced Circulation Liquid Lithium Loop (FCLLL-1).

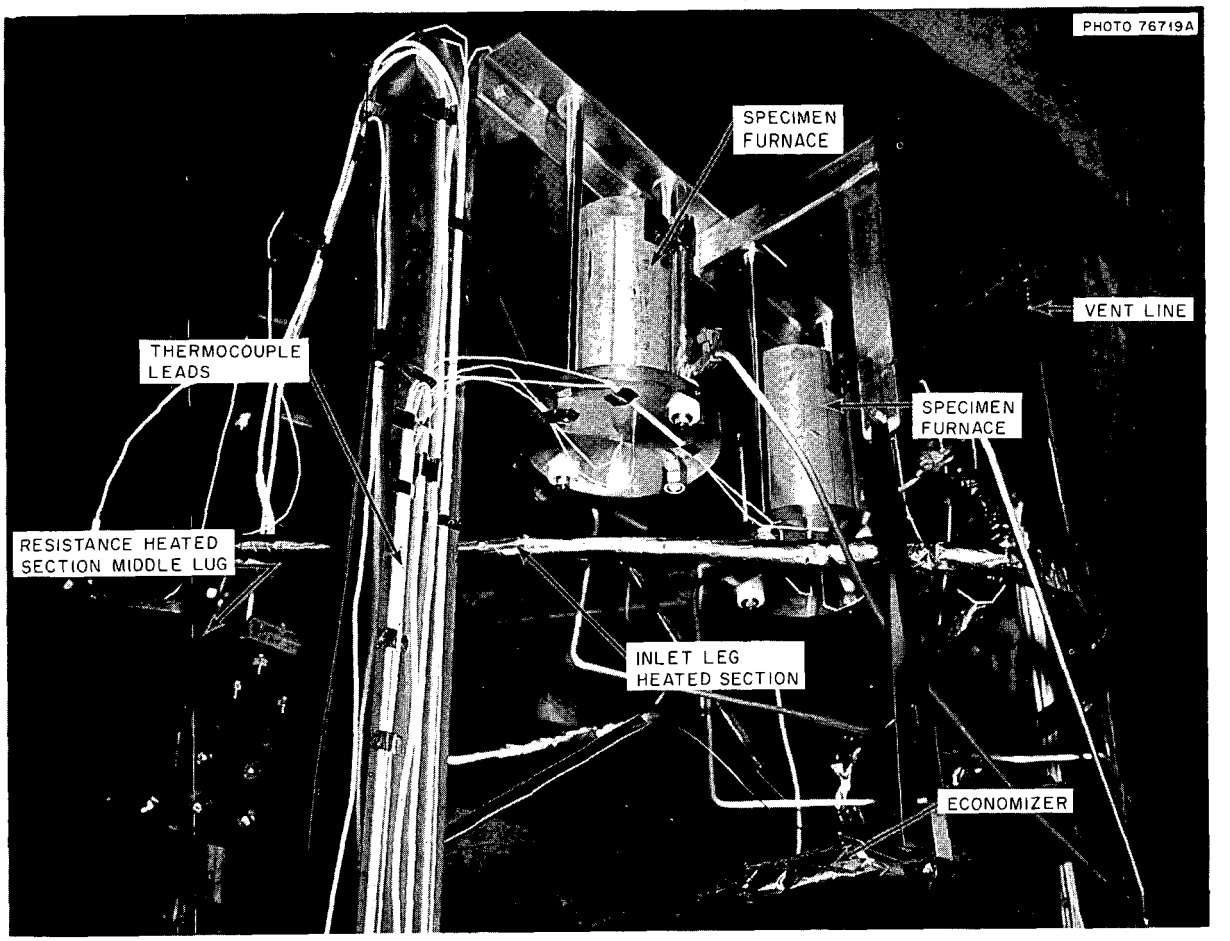

Fig. 5.13. Specimen Furnaces in Forced Circulation Liquid Lithium Loop (FCLLL-1).

which was 1/16 in. in diameter, was Ta near the hot-junction end and type 304 stainless steel beginning about 24 in. from the hot junction. We used BeO powder for insulation in the Ta section and MgO in the stainless steel section. The dissimilar sheath materials were joined by a brazed sleeve. The sheathed thermocouples that were attached to the resistance-heated section of the loop were threaded through BeO and Al_2O_3 beads to avoid short circuits to the support structure and the chamber.

Thermal Cycling Test. – Before filling the loop, we thermally cycled the resistance-heated section. The rate of heating was adjusted manually to limit the pressure in the vacuum chamber to below 1×10^{-5} torr. The temperature was increased in gradual increments to 1370°C and held for 2 hr. The loop was monitored for leaks throughout the thermal cycle by

pressurizing the loop internally to 0.8 torr with pure He and monitoring the gases in the vacuum chamber for He with a leak detector that has a sensitivity of 10^{-10} std cm^3/sec. The loop remained free of leaks during and after the thermal cycle.

Lithium Purification. — When we attempted to sample the Li drum originally purchased for this loop, we discovered a gas leak above the Li level. After repairing the leak, we sampled the Li through a 10-μm filter at 315°C. The analysis showed excess of 4000 ppm N and 125 ppm O. When the Li was sampled again at 205°C through a 10-μm filter, it showed a concentration of about 1200 ppm N. Although the purity was improved by the use of the lower filtration temperature, we still considered it unacceptable and ordered replacement. To expedite the order, we designed and built a new supply drum and shipped it to the vendor, who filled it with Li.

The concentrations of impurities as received in a Li sample taken from the replacement drum at 205°C through a 10-μm filter are shown in Table 5.9. We transferred 25.5 lb of this Li at 200°C to the system fill-and-drain tank for further purification. The tank, which contained Zr foil produced from high-purity crystal bar stock, was heated to a hot-trapping temperature of 815°C. A sample was taken after 40 hr at this temperature. The results, shown in Table 5.9, indicate that the purification treatment was very effective in lowering the levels of O and N.

The N and O concentrations in a subsequent sample of the Li used to flush the loop were also low (see Table 5.9), and the flush charge was approved for use without further purification.

Filling the Loop with Lithium. — In preparation for filling the loop with Li, we preheated the T-111 piping by radiation from the electrically-heated walls of the chamber bell and bowl. The temperature of the chamber wall was increased slowly (10°C/hr) to avoid temperature transients that could cause distortion of the main chamber flange and possible air leaks. The temperature was raised until the coldest point in the primary circuit of the loop (the flowmeter magnet) was just above the melting point of Li. The bypass circuit, most of which is outside the vacuum chamber, was heated with tubular electric heaters to a maximum temperature of 540°C to ensure that all points would be above the melting

Table 5.9. Chemical Analysis of Lithium Used in Forced Circulation Liquid Lithium Loop (FCLLL-1)

Element	Concentration, ppm		
	As Received	After Hot Trapping[a]	After Loop Flush[b]
O	48	12	9
		23	11
			16
N	201	< 5	< 5
	224	< 5	< 5
Ag	< 1	< 1	< 1
Al	< 10	< 10	< 10
B	< 1	< 1	< 1
Ba	< 5	< 5	< 5
Be	< 1	< 1	< 1
Bi	< 2	< 2	< 2
Ca	< 100	< 100	< 100
Cb	< 20	< 20	< 20
Co	< 5	< 5	< 5
Cr	5	5	5
Cu	10	10	10
Fe	50	50	20
Hf	< 20	< 20	< 20
K	30	30	30
Mg	≤ 1	≤ 1	≤ 1
Mn	3	7	2
Mo	≤ 1	< 1	< 1
Na	50	70	30
Ni	20	10	10
Pb	< 3	< 3	< 3
Sb	< 5	< 5	< 5
Si	≤ 5	≤ 5	≤ 5
Sn	< 3	< 3	< 3
Ta	< 20	< 20	< 20
V	< 3	< 3	< 3
W	< 20	< 20	< 20
Zr	< 20	< 20	< 20

[a]After hot trapping 40 hr at 815°C.

[b]Flushing consisted of more than 100 volume changes at 300°C in both the primary and bypass circuit over a period of 2 hr.

point of Li. The temperature of the Li in the fill-and-drain tank was adjusted to 315°C. The helical induction pump of the primary circuit was heated by operating it empty to maintain the reflective insulation around the pump at 315°C.

We added a total of 7.2 lb of Li to the primary and bypass circuits by pressurizing the fill-and-drain tank as necessary to maintain flow into the loop through the 10-μm filter at 315°C. We followed the movement of Li during filling by means of the continuous level recorder on the fill-and-drain tank, thermocouples, the flowmeters on the primary and bypass circuits, and the pressure recorder on the primary circuit.

Since the Li pump was already energized for preheating purposes, it immediately began circulating Li in the primary and bypass circuits. The Li inventory was maintained at a nearly constant temperature of 315°C by power input from the pump, the chamber heaters, and the bypass-circuit heaters.

The Li was circulated for 2 hr and then sampled (Table 5.9). The average temperature in the primary circuit was 300°C; the flow rates were 1.2 gpm in the primary circuit and 0.5 gpm through the bypass circuit. At least 100 volume changes were made in the primary circuit and 150 volume change units in the bypass circuit before sampling.

We maintained the temperature level in the loop by increasing the power to the pump and piping heater as the walls of the vacuum chamber were cooled. The chamber was slowly cooled at 5.5°C/30 min by reducing the power to the bakeout heaters for the vacuum chamber.

Trial Run. — The temperature of the Li in the primary circuit at the resistance-heater exit was increased in steps from 315°C to the design temperature of 1370°C. We experienced a number of thermocouple failures throughout the trial period, and many of the temperature data appeared questionable. Therefore, we terminated the trial run and opened the chamber to inspect and remedy the difficulties.

An inspection of the bare-wire thermocouples revealed that 8 of 12 had failed either because of shorting or breaking or detachment of the wires at their junctions with the loop piping. In the sheathed thermocouples, 5 of 11 sensing wires had broken at the transition joint in the sheath material, as shown in Fig. 5.14. The transition from Ta to

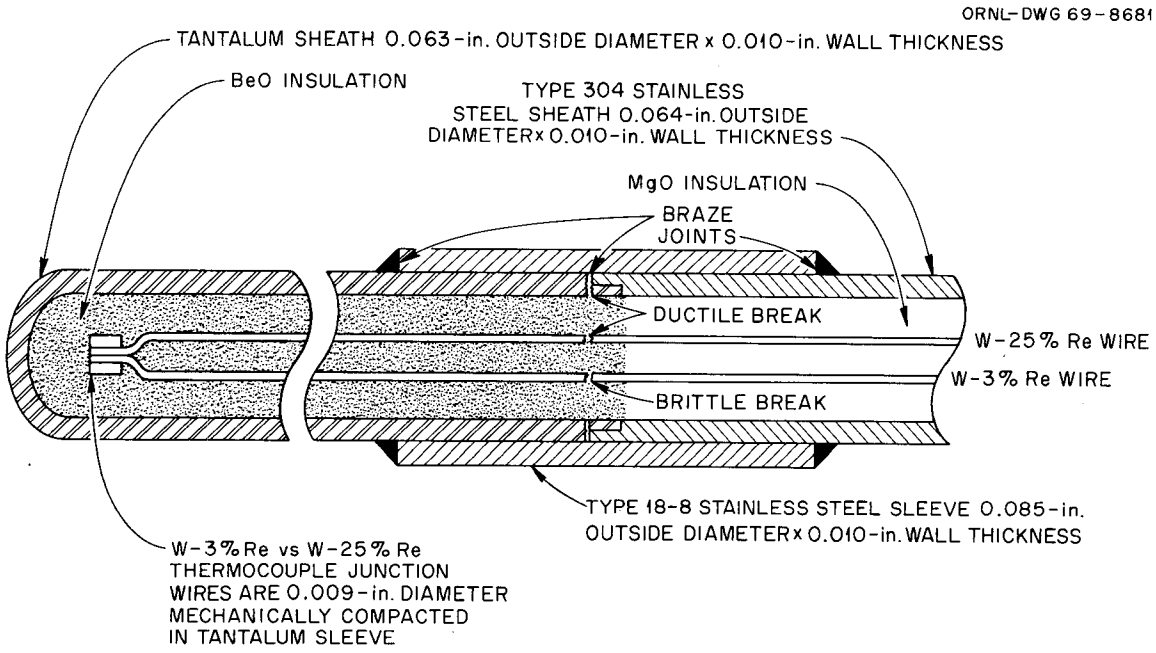

Fig. 5.14. Typical Thermocouple Failure Induced by Differential Thermal Expansion in Forced Circulation Liquid Lithium Loop Test (FCLLL-1).

stainless steel sheath material was adopted to reduce the cost of the thermocouple sheathing. Because the vendor's test experience had shown the original transition joint to be mechanically weak, a stainless steel sleeve was brazed over the joint for mechanical protection. Apparently, the differential thermal expansion between stainless steel and Ta was sufficiently great that the sheath joint and the wires were subjected to excessive tensile stresses when the sleeve temperature was increased by radiant heating. The reason for failure of the remaining six sheathed thermocouples is not clear and is still being investigated. Five of these thermocouples were found to have low resistance from wires to sheath near the hot junction.

The primary circuit was subjected to several thermal cycles as a result of normal heating and cooling operations and equipment difficulties. Four severe thermal cycles resulted from sudden restoration of power to the Li pump and the resistance-heated section after power failures. During the most severe of these cycles, the exit temperature in the resistance-heated section changed from 950 to 715°C at a rate estimated to be 3000°C/min. Thermal cycles were also experienced when

the heater power was lost because of problems in the control instrumentation and electrical power circuit. During the worst of these thermal cycles the temperature at the exit of the resistance-heated section dropped from 1290 to 925°C in 3 min. At lower temperatures, these thermal cycles were less severe: at 1066°C, a rate of drop of 27°C/min was observed; at 849°C, a rate of drop of 15°C/min was observed. The heating rates, in contrast, were no greater than 16°C/min.

We observed no damage to the loop piping as a result of these thermal cycles. However, we did observe failure of thermocouples throughout this period.

Vacuum Environment for Primary Circuit. — The major off-gas loads were encountered while the loop was being heated before it was filled with Li and when the primary circuit was being raised to design temperature. The chamber pressure peaked in the 10^{-4} torr range as the primary loop was heated preparatory to receiving the Li. The chamber pressure was held below 5×10^{-5} torr during subsequent heating of the primary circuit to the design conditions.

A diffusion pump with a liquid-N-cooled, optically baffled trap was used to handle the peak outgassing loads. The triode ion pumps were turned on and the diffusion pump valved off when the chamber had cooled and its pressure was near 5×10^{-6} torr. The loop was operated at 315°C. While the loop was being heated, the ion pumps developed Ar instabilities and control of the pressure in the chamber was returned to the diffusion pump. During one instability, the chamber pressure surged from 10^{-9} to 10^{-4} torr, and the safety circuits automatically cut off the ion pumps. A monopole type of gas analyzer identified Ar as the offending gas. The Ar source was traced to the dry box through which the bypass circuit passes. Argon entered the chamber through the porous ceramic of the tubular trace heaters used to heat the bypass plumbing. The loop temperature was reduced and maintained at 260°C, and the chamber was backfilled with dry N_2 while ceramic-metal seals were applied to the heater ends that terminated in the dry box. The diffusion pump and the ion pumps were operated together until the Ar instabilities disappeared.

Hydrogen constituted the principal gas impurity within the vacuum chamber during the period when the chamber walls were water cooled and the loop was being heated up to design conditions. Water vapor and organic materials were detected after the chamber bakeout period, but these disappeared with time. Two typical gas analyses are given in Table 5.10. During these analyses, the chamber pressure was maintained by the diffusion pump alone.

Table 5.10. Typical Analysis of Residual Gas During Trial Run Period of Forced Circulation Liquid Lithium Loop Test (FCLLL-1)

Residual Gas	Composition, ppm	
	During Heating to 1075°C[a,b]	After Heating to 1315°C and Cooling to 980°C[a,c]
H_2	2000	80
CH_4	89	1
H_2O	35	< 1
N_2,CO	170	8
O_2	1	< 1
Ar	7	< 1
CO_2	80	< 1

[a]The component peak current values are roughly proportional to the component partial pressures.

[b]Total pressure of 5.1×10^{-6} torr, peak current of 10^{-9} amps.

[c]Total pressure of 4.4×10^{-7} torr, peak current of 10^{-9} amps.